Geomechanics and Engineering, *Vol. 27, No. 4 (2021) 309-322*
https://doi.org/10.12989/gae.2021.27.4.309

Effect of freeze-thaw cycles on the mechanical properties and constitutive model of saline soil

Shukai Cheng[1], Qing Wang*[1], Huicheng Fu[2], Jiaqi Wang[1], Yan Han[1], Jiejie Shen[1] and Sen Lin[2]

[1]*College of Construction Engineering, Jilin University, Changchun 130012, Jilin, China*
[2]*Jilin Provincial Water Resources Department, Changchun, Jilin, China*

(*Received October 11, 2020, Revised October 12, 2021, Accepted October 18, 2021*)

Abstract. The freeze-thaw cycle is one of the most common natural physical processes in cold regions and will significantly affect the deformation characteristics of saline soil. To study the mechanical properties and constitutive relationship of saline soil under freeze-thaw cycles, in this paper, a series of freeze-thaw cycle tests and consolidated-drained (CD) triaxial tests were conducted on remodeled saline soil in the Qian'an area of western Jilin, China. Based on the elliptic-parabolic double yield surface constitutive model, a modified model considering the effects of freeze-thaw cycles is established. The results show that the specimen exhibits a strain-hardening stress-strain relationship, and the volumetric strain during shearing exhibits a shear-shrinkage characteristic overall. As the number of freeze-thaw cycles increases, the volumetric strain gradually increases, and the shear strength gradually decreases. As the confining pressure increases, the volumetric strain gradually increases. Then, the elliptic function and parabolic function are selected to describe the volume yield surface and the shear yield surface on the p-q plane respectively. By introducing the correlation flow rule, the functional relationship between the deviating stress increment and the axial strain increment and volumetric strain increment is derived. Based on the results of the triaxial test, the variation in the model parameters with the number of freeze-thaw cycles was determined. The results show that as the number of freeze-thaw cycles increases, c, φ, h, K, n, M_1, M_2, and a show a decreasing rule, while t shows a gradually increasing rule, and all factors can use logistic function to fit the regression relationship between the model parameters and the number of freeze-thaw cycles. The expression of the model parameters with the number of freeze-thaw cycles as a factor is substituted into the stress-strain increment constitutive equation, and a modified double yield surface model considering the effects of freeze-thaw cycles is established. The calculated values of the model are basically consistent with the measured values. This shows that the double yield surface constitutive model can be applied to saline soil.

Keywords: consolidated-drained triaxial test; double yield surface model; freeze-thaw cycle; model parameters; saline soil; stress-strain relationship

1. Introduction

Shallow foundations of various engineering projects undergo repeated freeze-thaw cycles due to the positive and negative temperature changes in cold regions, which in turn cause various engineering disease problems. With the development of railways, highways, power stations and diversion irrigation projects, frozen soil in cold regions is widely used as the foundation and structure of the project (Hu *et al.* 2021, Li *et al.* 2017, Suebsuk *et al.* 2019, Yu *et al.* 2016, Zhang *et al.* 2012). The design and maintenance of these projects require a deep understanding of the strength and deformation characteristics of the soil under freeze-thaw cycles (Liu *et al.* 2014, Wang *et al.* 2018, Zhou *et al.* 2015, Zhu *et al.* 2016) and are also deeply affected by geological conditions (Bai *et al.* 2021, Cheng *et al.* 2021). The constitutive model can perform quantitative strength and deformation calculations, and establishing a constitutive model considering the effects of freeze-thaw cycles is one of the important contents of geotechnical engineering research in cold regions.

The constitutive model of soil mainly includes a nonlinear elastic model and elastoplastic model. Nonlinear elastic models include Duncan-Zhang *E-v*, *E-B* models and *K-G* models (Duncan and Chang 1970), but such models cannot reflect the shear dilatancy and the cross-effect of compression and shear. The elastoplastic model mainly refers to the Cambridge model (Roscoe and Schofield 1963) proposed by Roscoe, and a series of single yield surface models developed on this basis. Asoka *et al.* (2000) established a revised model that reflects historical dependence and structure by embedding overconsolidation parameters and structural parameters in the yield function of the Cambridge model and forming up and downloading in the *p-q* space yield surface. Based on the state-dependent dilatancy theory, the parameters related to the characteristic state stress ratio and the peak stress ratio are introduced to establish a model that can describe the dependence of soil shear and dilatation density (Li and Dafalias 2000). Huang *et al.* (1981) and Li (2006) established and improved the Tsinghua model and determined the direction of the plastic strain increment under various stress states through experiments, the yield surface according to the associated flow law, and then the hardening parameters from the test results. Yao (2015) proposed a UH model for

*Corresponding author, Ph.D., Professor
E-mail: wangqing@jlu.edu.cn

ISSN: 2005-307X (Print), 2092-6219 (Online)

overconsolidated soil and normal-consolidated soil based on the Cambridge model and the concept of a lower loading surface. The single yield surface model is a "hat" model. The limitation to this model is that it can only reflect the characteristics of shear, and there may still be yielding within the yield surface in the stress space. For this reason, double yield surface and multiple yield surface models have been developed. Lade (1977) first explained the meaning of the double yield surface, defining the volumetric yield surface as the failure yield surface, the shear yield surface as the plastic expansion yield surface, and the latter as the bullet-shaped cone surface. Shen (1980) combines the advantages of the Duncan-Zhang model and the Cambridge model to establish a double-yield "south water" model that can simulate the stress path characteristics of decreasing confining pressure or average pressure. Yin (1988) (1996) proposed a yield function and a hardening function related to compression and shear, respectively, and used the associated flow rule to establish another model of a double yield surface. Huang *et al.* (2008) introduced shape parameters into the Cambridge model and established a double-yield surface model that reflects strain softening through a strain softening formula that utilizes the residual stress ratio and peak stress ratio. In addition, some constitutive models, such as the classical yield surface model, the boundary surface theoretical model, and the internal time model have also been proposed (Yao *et al.* 2012). At present, many studies have shown that for geotechnical materials, the single yield surface model (associated and nonassociated) has difficulty to accurately describing its mechanical and deformation characteristics, and the double-yield surface model considering both shear and volume deformation characteristics has been widely used and recognized (Lai *et al.* 2010, Liu *et al.* 2012, Zhao *et al.* 2019).

Constitutive models are one of potential research direction to develop and verify the applicability of constitutive models of different soils in various environments and under distinct boundary conditions. In terms of the deformation characteristics of frozen soil, there have been various forms of viscoelastic-plastic and elastoplastic damage models (Lai *et al.* 2009, Lai *et al.* 2014). At the same time, irreversible deterioration after frozen soil thaws is also the main cause of engineering discrepancies in cold regions, and some constitutive models have been established to consider the effects of freeze-thaw cycles. Liu *et al.* (2016) proposed new normalization factors based on the hyperbolic model, including ultimate partial stress and freeze-thaw cycle damage coefficient, to predict the stress-strain relationship of soil under freeze-thaw cycles. Cui *et al.* (2015) fit the volume and shear yield surface on the *p*-*q* plane with elliptic and parabolic equations respectively, expressed the volume and shear hardening functions as logarithmic functions and exponential functions, and reflected the influence of freeze-thaw cycles by describing the changing law of the hardening function coefficients. Chang *et al.* (2015) (2016) describe the volume and shear yield surfaces as elliptic and linear functions, and the volume and shear hardening functions as logarithmic and hyperbolic functions. The coefficients are fitted to a cubic polynomial with the number of freeze-thaw cycles as a factor, and a double-yield surface model considering freeze-thaw cycles is established. Hu *et al.* (2019) used elliptic and parabolic functions to describe volume and shear yield surfaces and established a double yield surface constitutive model of silty clay considering the effects of freeze-thaw cycles. Studies by many scholars have shown that it is feasible to describe the effects of freeze-thaw cycles on soils by selecting reasonable yield surfaces, hardening functions, and expression coefficients of hardening functions based on the classic two-yield constitutive model (Chang and Lai 2018, Chen and Zhu 2016, Kong *et al.* 2017, Sukkarak *et al.* 2016, Zhang *et al.* 2018, Zhou and Zhu 2010).

For the saline soil in the cold regions, the presence of salt in the soil makes the water in the soil have a more pronounced effect on the physical and mechanical properties of the soil during the process of the environmental temperature. Many studies have been conducted on carbonated saline soil in western Jilin Province. Wang *et al.* (2016) proposed that the saline soil here is a structural soil. In terms of dispersibility, Bao *et al.* (2013) and Zhang *et al.* (2015) studied the dispersion characteristics of the area and considered the saline soil in the area to be a disperse saline soil. Zhang *et al.* (2021) studied the water-heat-salt-mechanical interaction of saline soil. In terms of mechanical properties, Han *et al.* (2018) studied the unconsolidated and undrained shear strength of saline soil in western Jilin under freeze-thaw cycles. Regarding the constitutive relationship of saline soil, Chang *et al.* (2019) studied the elastoplastic constitutive model of grain crushing of frozen salt coarse sand. Yang *et al.* (2019) studied the constitutive model of saline soil corroding concrete under uniaxial compression. Zhao *et al.* (2020) studied the boundary surface constitutive model of frozen saline silt under cyclic loading. However, there are relatively few studies on the constitutive relationship of carbonated saline soil under freeze-thaw cycles. With the continuous development of various engineering constructions, saline soil is increasingly used as the foundation for various projects. In cold regions, the applicability of the freeze-thaw cycle effect of the constitutive model of saline soil also needs further analysis. It is of great theoretical and practical significance to study the constitutive model of saline soil under freeze-thaw cycles for the study of engineering stability in cold regions.

In this paper, a series of freeze-thaw cycle tests and consolidated-drained triaxial tests were conducted on saline soil in the Qian'an area of western Jilin. Based on Yin Zongze's elliptic-parabolic double yield surface constitutive model, the experimental results of the relationship between deviatoric stress-axial strain-volume strain are analyzed. Then the change rule and regression relationship of each model parameter with the number of freeze-thaw cycles were determined. Finally, a modified double yield surface model considering the effects of freeze-thaw cycles is established. The modified double yield surface constitutive model provides a theoretical basis for the engineering construction of saline soil areas in cold regions.

2. Materials and experimental program

2.1 Materials

Western Jilin, China, is a typical seasonal frozen soil region, and it is also the main saline soil distribution area.

Table 1 Basic physical properties of natural saline soil

Soil type	Natural density(g/cm^3)	Specific gravity of solid Particles(g/cm^3)	Plastic limit (%)	Liquid limit (%)	Optimum water content (%)	Maximum dry density(g/cm^3)
CL	1.97	2.72	17.18	24.98	15.6	1.78

Table 2 Basic chemical properties of natural saline soil

Item	Soluble salt content (%)	K^+ (mmol/kg)	Na^+ (mmol/kg)	Ca^{2+} (mmol/kg)	Mg^{2+} (mmol/kg)	SO_4^{2-} (mmol/kg)	HCO_3^- (mmol/kg)	Cl^- (mmol/kg)
Content	0.55	1.22	31.46	1.42	2.4	0.25	3.76	1.47
Method	Water-bath evaporation	Flame photometer		EDTA complexometric titration			Neutralization titration	Silver nitrate titration

Note: Each item was measured with the filtrate of 1:5 soil-water extractives.

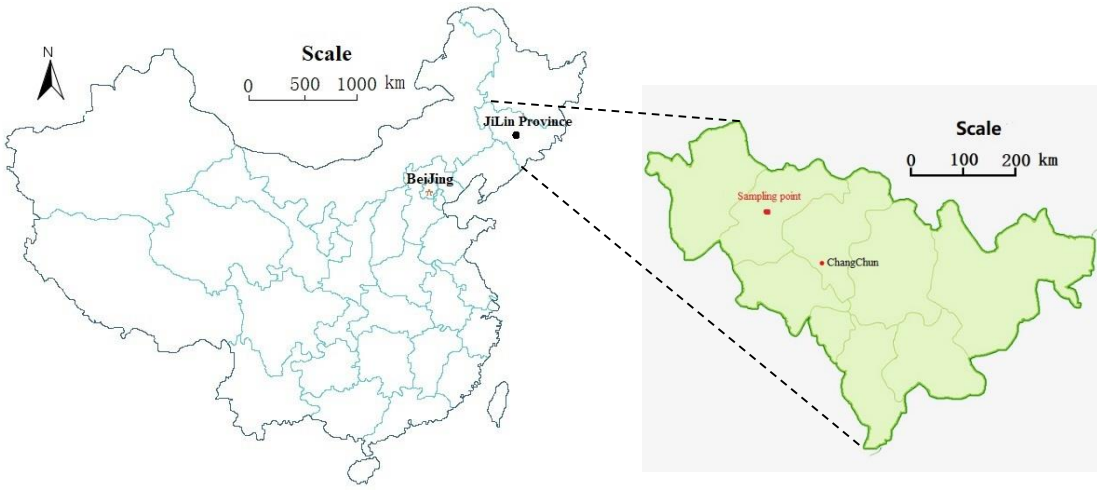

Fig. 1 Geographical location of sampling point

Qian'an County is a typical saline soil distribution area and the specific sampling point location is shown in Fig. 1. The saline soil in this area has a significant dispersivity and is prone to damage under the action of water (Zhang *et al.* 2015). The average annual evaporation in this area is much larger than the annual average precipitation, which accelerates the formation of salinization. Under the combined action of infiltration and evaporation, the salt content is highest at a depth of 40 cm. Therefore, the experimental soil samples for this research were taken from a depth of 40 cm in Qian'an County. The basic physical and chemical properties of the soil are listed in Table 1 and Table 2, respectively. The physical parameters (grain size distribution) of saline soil are shown in Fig. 2. From its physical property parameters, saline soil here was classified as lean clay (CL) based on the Unified Soil Classification System (USCS) (ASTM 2011).

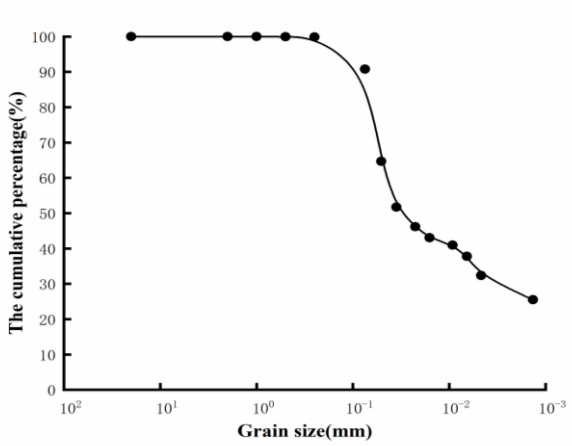

Fig. 2 Grain size distribution of natural saline soil

2.2 Specimen preparation

The soil samples taken from the experimental site were dried and then passed through a 2 mm sieve. Water was added according to the optimal moisture content in the soil, mixed it and allowed to stand for 24 hours to evenly mix the water. Then, using a molding machine, a standard triaxial specimen with a diameter of 39.1 mm and a height of 80 mm was prepared. In engineering practice, the degree of compaction is generally not less than 90%; therefore, the compactness was controlled to 90%. According to the basic properties of the test soil sample and the controlled compaction, the calculation can be obtained: the dry density of the triaxial sample is 1.603 g/cm^3, the initial saturation is 60.88%, with porosity of 0.70. After the specimen is made, it is wrapped and sealed with a plastic film to simulate a closed system without an external water supply.

2.3 Experimental scheme

The number of freeze-thaw cycles and confining pressure were selected as test variables to conduct a

Table 3 Experimental scheme of the test

Moisture content (%)	Degree of compaction (%)	Freeze-thaw cycles	Confining pressure σ_3 (kPa)
15.6	90	0(FT0) 1(FT1) 10(FT10) 30(FT30) 60(FT60) 90(FT90) 120(FT120)	50 100 200 300

comprehensive test of two factors. A simulation platform for freeze-thaw testing of rock and soil in an ultracold environment was used in this study. According to the seasonal average temperature of the soil samples and the common freeze-thaw cycle test conditions, the experimental freezing temperature was set to -20 °C, and the melting temperature was set to 20 °C. The freezing time was set to 12 h, and the melting time was also set to 12 h to ensure that the sample is completely frozen and fully thawed. Completing one freezing process and melting process is one freeze-thaw cycle. Freeze-thaw cycles of specimens were set to 0, 1, 10, 30, 60, 90 and 120, and corresponding soil specimens were designated FT0, FT1, FT10, FT30, FT60, FT90 and FT120 to simulate the various freeze-thaw cycles. After the desired number of designed freeze-thaw cycles is attained, the specimens are removed for consolidated-drained triaxial tests, and the remaining soil specimens continue to be subjected to freeze-thaw cycles. The specific experimental scheme is shown in Table 3.

The test was conducted on a strain-controlled triaxial test apparatus (model TSZ-3, manufactured by Nanjing Soil Instrument Factory Co., Ltd., Nanjing, China). Effective consolidation pressure was selected at four levels of 50, 100, 200 and 300 kPa for a total of 28 groups of tests. The test steps are as follows: First, the triaxial sample that has reached the set number of freeze-thaw cycles from the freeze-thaw instrument for vacuum saturation is removed, and the saturation can reach more than 95%. Then, the saturated triaxial sample is installed in the triaxial instrument, and the isotropic consolidation process is conducted under an effective consolidation pressure. Finally, keep the confining pressure constant after consolidation, keep open the drain valve, perform a drained shear test at an axial rate of 0.01 mm/min, and end the strain control to 16%.

3. Results and discussion

3.1 Stress-strain relationship

According to the recommended method of the "Geotechnical Test Method Standard", the deviator stress and volumetric strain are calculated by comprehensively considering the volume change during the freeze-thaw cycle, consolidation and shearing process. The deviator stress-axial strain curves under different test conditions are shown in Fig. 3. The stress-strain curves of the samples all show strain hardening, and the deviator stress gradually increases with increasing axial strain. As the shear stress increases, the specimen will eventually undergo plastic failure. The stress-strain curve can be divided into three stages: the quasi-elastic stage, strain hardening stage, and failure stage. The appearance of the yield point is more pronounced, which occurs between 3% and 5% of the axial strain. At the same time, the position of the stress-strain curve gradually decreases with the increase in the number of freeze-thaw cycles; that is, the deviator stress corresponding to the same axial strain gradually decreases with the increase in the number of freeze-thaw cycles.

The criterion for determining the shear strength in the strain hardening stress-strain curve is to take the deviator stress value corresponding to 15% of the axial strain. The change in shear strength under various test conditions is shown in Fig. 4. As the number of freeze-thaw cycles increases, the shear strength gradually decreases. At the same time, the rate of decline before 10 freeze-thaw cycles is larger, and the strength of the soil is still declining after 10 freeze-thaw cycles, but the rate of decline is slower than before 10 freeze-thaw cycles. This is because the pore water freezes into ice during the freezing process of the soil, and the pore volume increases. Under the action of salt, the volume increases more significantly, and the expanded pores remain in place during the melting process. After 10 freeze-thaw cycles, larger pores can be connected into linear cracks. Therefore, the strength decreases rapidly after the first 10 freeze-thaw cycles. With the increase in the number of freeze-thaw cycles, the development of cracks becomes slower. Therefore, during the 30-120 freeze-thaw cycles, the strength decrease becomes slower. However, it can also be seen from Fig. 4 that as the freeze-thaw cycle increases, the strength continues to decrease, indicating that the freeze-thaw cycle has a continuous deteriorating effect on the strength of the saline soil.

3.2 Volumetric strain characteristics

In the consolidated-drained triaxial test, in the consolidation stage, the drained volume of the specimen after various freeze-thaw cycles are shown in Table 4. It can be seen that the consolidated drained volume gradually increases with the increase in the number of freeze-thaw cycles or confining pressure. The reason is that in the freezing process, the pore water of the sample freezes into ice, and the volume increases. Under the action of salt, the frost heave effect is more significant, and the frost heave effect will rupture the internal structure and connection of the soil. In the process of melting, the soil structure cannot be completely restored, which shows the phenomenon of volume increase in the macroscopic view. Therefore, under the same consolidation confining pressure, the consolidation drainage of the sample gradually increases with increasing freeze-thaw cycles. Under the same number of freeze-thaw cycles, as the consolidation confining pressure increases, the compaction effect on the soil is enhanced. As the confining pressure increases, the consolidation drainage volume also increases.

In the shear stage, the relationship between volumetric strain and axial strain under separate test conditions are shown in Fig. 5. Fig. 5 shows that the volumetric strain exhibits shrinkage. It can be seen from the stress-strain

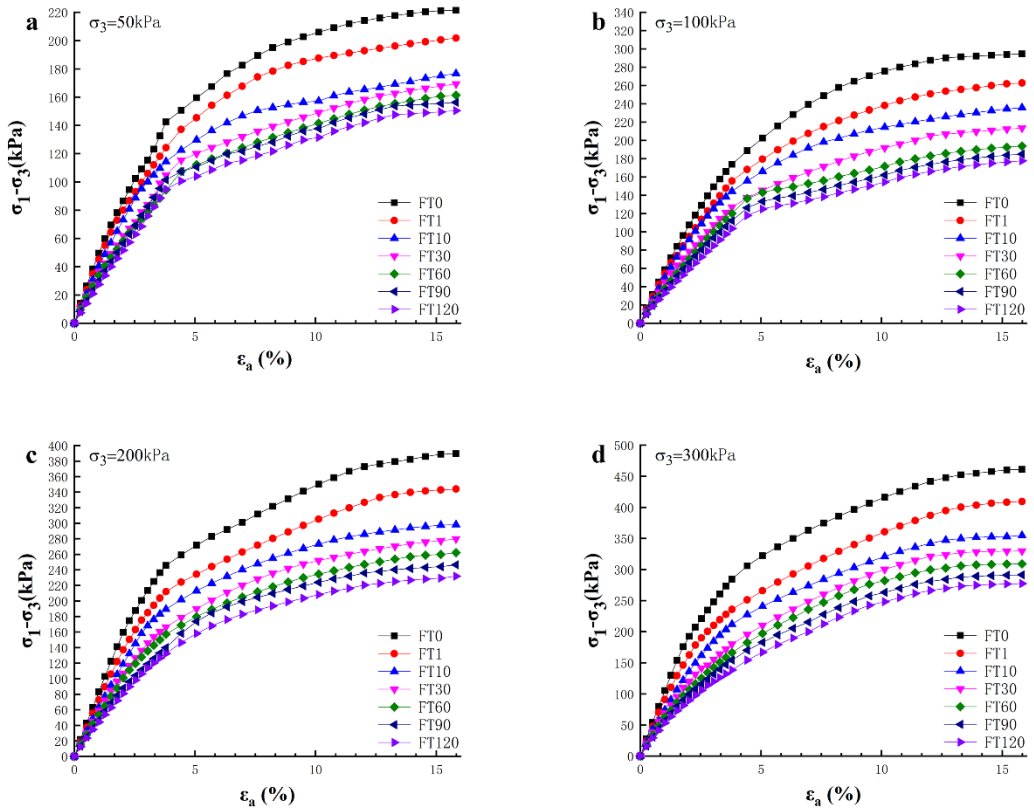

Fig. 3 Deviatoric stress-axial strain behavior of specimens under different freeze-thaw cycles and confining pressures

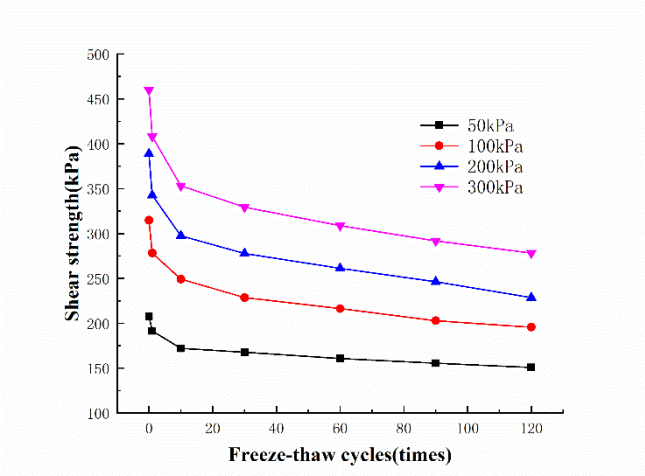

Fig. 4 The change in shear strength under various test conditions

Table 4 The consolidated displacement of specimen under different test conditions(cm^3)

confining pressure （kPa)	50	100	200	300
FT0	3.3	4.3	5.4	6.6
FT1	3.4	4.5	5.6	6.7
FT10	3.5	4.7	5.8	6.9
FT30	3.6	4.8	6.1	7.1
FT60	3.6	5	6.3	7.4
FT90	3.8	5.1	6.4	7.7
FT120	3.9	5.3	6.6	7.8

curve of remolded saline soil that the curve has a clear yield point and belongs to the strain hardening type, indicating that the curve exhibits compressive hardening, so the volumetric strain reflects the characteristics of shrinkage. As the confining pressure increases, the volumetric strain gradually increases. At the same time, as the number of freeze-thaw cycles increases, the volumetric strain corresponding to the same axial strain also gradually increases. The specimen essentially shows shear shrinkage. Under the same test conditions, the volumetric strain gradually increases with increasing axial strain. When the confining pressure is low, the shear dilatation phenomenon occurs at the end of the shearing stage, and as the number of freeze-thaw cycles increases, this phenomenon gradually weakens and disappears. The main reason is that under the same consolidation confining pressure, as the number of freeze-thaw cycles increases, the pores between the soil particles are larger, and the degree of consolidation continues to decrease. The soil was in a compact state during the shearing process. Therefore, the dilatancy at the end of the shear phase gradually weakened. Comparing Figs. 5 (a)-(d), it can be seen that under the same number of freeze-thaw cycles, with increasing confining pressure, the dilatancy at the end of the shearing stage continuously weakens and disappears. The main reason is whether the confining pressure is sufficient to hinder the rolling friction

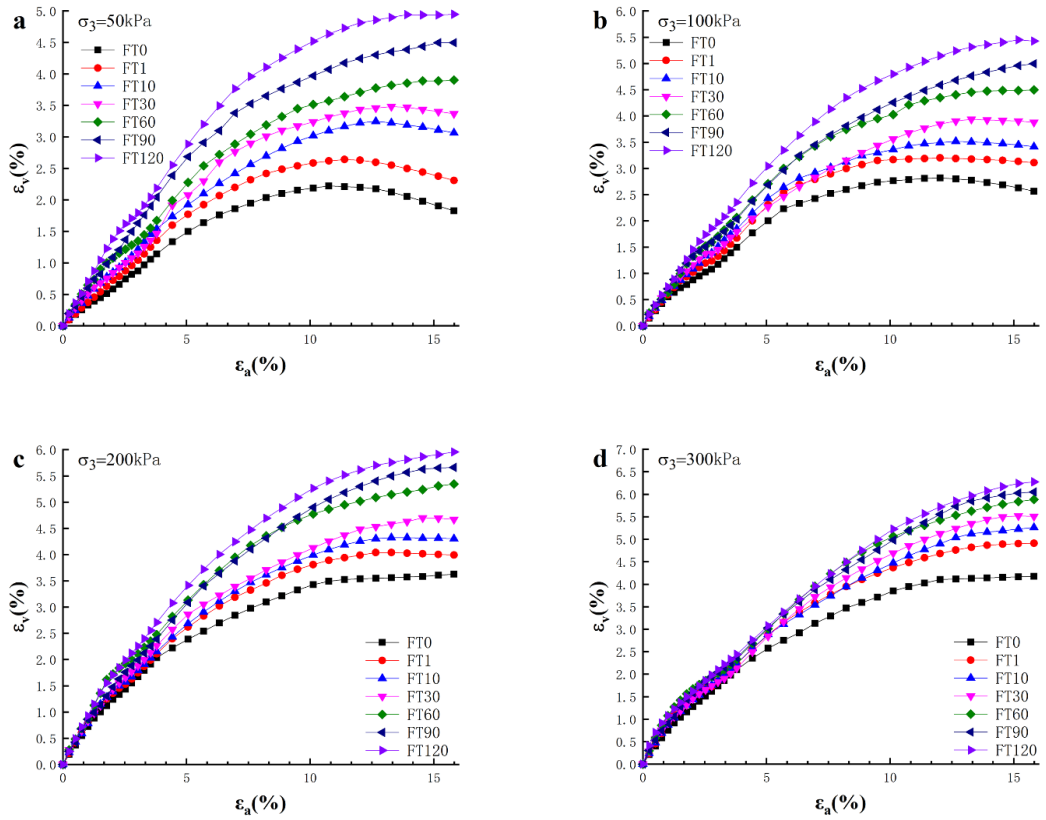

Fig. 5 Volumetric strain-axial strain behavior of specimens under different freeze-thaw cycles and confining pressures

between the particles under the same number of freeze-thaw cycles. If the confining pressure is large, it has a strong inhibitory effect on the expansion of the soil in the shearing process; then, there is only sliding friction between the particles, and the volume will not increase. If the confining pressure is too small, its inhibitory effect becomes weak, and rolling friction will occur between the particles during the shearing process, resulting in a certain amount of shear expansion.

4. Ellipse-parabolic double yield surface model and parameter determination

4.1 Ellipse-parabolic double yield surface model

In the elliptic-parabolic double yield surface model (Yin 1988, Yin *et al.* 1996), the yield surface is regarded as the boundary of the elastic region, which consists of an elliptic function and a power function. Soil deformation includes elastic deformation $d\varepsilon^e$ and plastic deformation $d\varepsilon^p$. Under the action of external force, the plastic deformation of the soil is related to the mutual displacement of the soil particles. When the soil particles are displaced with each other, some of them fall into the original pores, causing volume shrinkage, and some will warp, causing volume expansion. Therefore, plastic deformation can be composed of two parts: $d\varepsilon_v^p$ and $d\varepsilon_s^p$, where $d\varepsilon_v^p$ is related to compression and $d\varepsilon_s^p$ is related to expansion, and it is

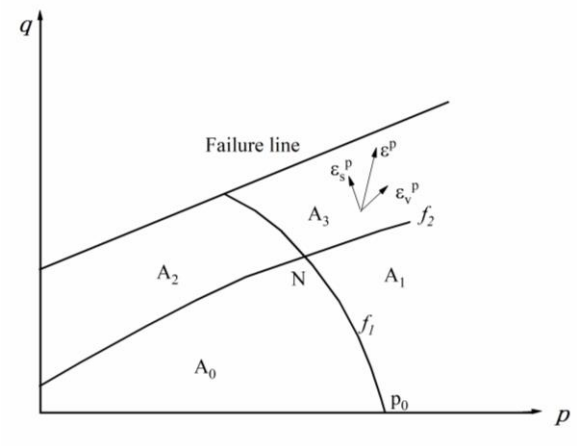

Fig. 6 Elliptic-parabolic yield surfaces model

assumed that both plastic deformations use the associated flow rule. As shown in Fig. 6, f_1 and f_2 represent the yield trajectory and p_0 is the abscissa of the intersection point of the yield locus f_1 and the p-axis. N represents the current point, and the p-q plane is divided into four regions: A_0, A_1, A_2, and A_3. A_0 has only elastic strain, A_1 is the plastic zone related to compression yield only, A_2 is the plastic zone related to expansion yield only, and A_3 is the plastic zone related to both yields. The direction of the N-point plastic increment is the vector accumulation of the plastic strain increment under each mechanism. The composition of the total strain $d\varepsilon$ is as follows:

$$d\varepsilon = d\varepsilon^e + d\varepsilon_v^p + d\varepsilon_s^p \tag{1}$$

4.1.1 Yielding associated with compression and expansion

The yield surface corresponding to compression adopts the elliptical shape in the modified Cambridge model, and the improved yield Equation f_1 is still in the form of an elliptic function. The main equations and parameters of the model are as follows(Yin 1988, Yin *et al.* 1996):

$$f_1(\sigma_{ij}, H_a) = p + \frac{q^2}{M_1^2(p + p_r)} - H_{a1}(\varepsilon_v^p) = 0 \tag{2}$$

In the formula, M_1 is related to the shape of the stress-strain curve, which is used to reflect the change in ellipse shape. p is the average normal stress and q is the generalized shear stress. ε_v^p is the hardening parameter of the elliptical yield surface. p_r is the intercept of the failure line on the p-q plane on the p-axis. H_{a1} is the hardening function corresponding to the compression yield surface. The p_r calculation formulas are as follows:

$$p_r = c\ \cot\varphi \tag{3}$$

where p_0 is the abscissa of the intersection point of the yield locus f_1 and the p-axis. The relationship between p_0 and ε_v^p under the three-axis isostatic test can be expressed in hyperbolic form, so the hardening function corresponding to the first yield surface is as follows:

$$H_{a1}(\varepsilon_v^p) = p_0 = \frac{h\varepsilon_v^p}{1 - t\varepsilon_v^p} p_a \tag{4}$$

where: h and t are dimensionless parameters describing the relationship between confining pressure and plastic volumetric strain. p_a is the standard atmospheric pressure, and the value is 101.3 kPa.

The yield Equation f_2 corresponding to the shear expansion is in the form of a parabolic function:

$$f_2(\sigma_{ij}, H_a) = \frac{aq}{G}\sqrt{\frac{q}{M_2(p + p_r) - q}} - H_{a2}(\varepsilon_s^p) = 0 \tag{5}$$

In the formula, a represents the proportion of the strain corresponding to the yield surface f_2 in the total plastic strain, and a higher a value corresponds to the dilatancy. G is the elastic shear modulus. ε_s^p is the hardening parameter of the parabolic yield surface. H_{a2} is the hardening function corresponding to the shear expansion yield surface.

The calculation formula of G is:

$$G = \frac{E}{2(1 + \mu)} \tag{6}$$

Approximately take the elastic modulus $E=2.0E_i$. Since the elastic strain accounts for a small proportion of the total strain, Poisson's ratio takes a constant of *0.3*. The initial tangent modulus E_i is related to the confining pressure, and the empirical relationship suggested by Janbu is:

$$E_i = kp_a\left(\frac{\sigma_3}{p_a}\right)^n \tag{7}$$

In the formula, p_a is the standard atmospheric pressure, and the value is 101.3 kPa. k and n are the intercept and slope of the line $lg(E_i/p_a)$ ~$lg(\sigma_3/p_a)$, respectively.

The hardening function corresponding to the second yield surface is as follows:

$$H_{a2}(\varepsilon_s^p) = \varepsilon_s^p = \int d\varepsilon_s^p = \int \frac{\sqrt{2}}{3}\sqrt{(d\varepsilon_1^p - d\varepsilon_2^p)^2 + (d\varepsilon_2^p - d\varepsilon_3^p)^2 + (d\varepsilon_3^p - d\varepsilon_1^p)^2} \tag{8}$$

4.1.2 Incremental constitutive equation

According to Eq. (1), the strain components include three parts: elastic strain component, compression-related strain component and expansion-related strain component. Next, the three strain components are solved separately.

First solve for the elastic strain component: where the elastic strain component $d\varepsilon^e$ includes volumetric elastic strain increment $d\varepsilon_v^e$ and generalized shear elastic strain increment $d\varepsilon_s^e$. The calculation formulas are:

$$d\varepsilon_v^e = \frac{dp}{K} = \frac{3(1 - 2\mu)dp}{2G(1 + \mu)} \tag{9}$$

$$d\varepsilon_s^e = \frac{dq}{3G} \tag{10}$$

In the formula, K represents the bulk modulus, and G represents the elastic shear modulus.

Second, the strain component related to compression is solved: the plastic strain related to compression consists of two parts: volumetric plastic strain increment $d\varepsilon_v^{p1}$ and generalized shear plastic strain increment $d\varepsilon_s^{p1}$. The Eq. (2) is fully differentiated to obtain:

$$\frac{\partial f_1}{\partial p}dp = dp/K_1 = \left(1 - \frac{q^2}{M_1^2(p + p_r)^2}\right)dp \tag{11}$$

$$\frac{\partial f_1}{\partial q}dq = dq/G_1 = \frac{2q}{M_1^2(p + p_r)}dq \tag{12}$$

$$\frac{\partial H_{a1}(\varepsilon_v^{p1})}{\partial \varepsilon_v^{p1}}d\varepsilon_v^{p1} = md\varepsilon_v^{p1} = \frac{hp_a + t\left[p + \frac{q^2}{M_1^2(p + p_r)}\right]}{hp_a}d\varepsilon_v^{p1} \tag{13}$$

Assuming that both yield surfaces apply the associated flow rule, we can obtain:

$$\frac{d\varepsilon_s^{p1}}{d\varepsilon_v^{p1}} = H_1 = \left.\frac{\partial f_1}{\partial q}\right/\frac{\partial f_1}{\partial p} = \frac{2q(p + p_r)}{M_1^2(p + p_r)^2 - q^2} \tag{14}$$

According to Eqs. (2) and (11)-(14), the calculation formulas for the volumetric strain increment $d\varepsilon_v^{p1}$ and the shear strain increment $d\varepsilon_s^{p1}$ can be obtained:

$$d\varepsilon_v^{p1} = \frac{dp/K_1 + dq/G_1}{m} \tag{15}$$

$$d\varepsilon_s^{p1} = \frac{dp/K_1 + dq/G_1}{m} \times H_1 \tag{16}$$

Finally, the strain increment related to expansion is solved: the plastic strain related to expansion includes the volumetric strain increment $d\varepsilon_v^{p2}$ and the shear strain increment $d\varepsilon_s^{p2}$. The solution method is the same as that of strain related to compression:

$$\frac{\partial f_2}{\partial p} dp = dp/K_2 = \frac{a}{2G} \cdot \frac{-q^{3/2}}{[M_2(p-p_r)-q]^{3/2}} dp \tag{17}$$

$$\frac{\partial f_2}{\partial q} dq = dq/G_2 = \left(\frac{a}{G} \cdot \sqrt{\frac{q}{M_2(p+p_r)-q}} + \frac{a}{2G} \cdot \frac{q^{1/2}(P+p_r)}{[M_2(p-p_r)-q]^{3/2}} \right) dq \tag{18}$$

$$\frac{d\varepsilon_v^{p2}}{d\varepsilon_s^{p2}} = H_2 = \frac{-M_2 q}{3M_2(p+p_r)-2q} \tag{19}$$

According to Eqs. (5) and (17)-(19), the calculation formulas for the volumetric strain increment $d\varepsilon_v^{p1}$ and the shear strain increment $d\varepsilon_s^{p1}$ can be obtained respectively:

$$d\varepsilon_s^{p2} = K_2 dp + G_2 dq \tag{20}$$

$$d\varepsilon_v^{p2} = (K_2 dp + G_2 dq) \times H_2 \tag{21}$$

According to classical elastoplastic theory, $d\varepsilon_v$ and $d\varepsilon_s$ can be obtained as follows:

$$\begin{Bmatrix} d\varepsilon_v \\ d\varepsilon_s \end{Bmatrix} = \begin{bmatrix} A_1 = 1/K + \frac{1}{mK_1} + H_2/K_2 & A_2 = \frac{1}{mG_1} + H_2/G_2 \\ A_3 = \frac{H_1}{mK_1} + 1/K_2 & A_4 = 1/3G + \frac{H_1}{mG_1} + 1/G_2 \end{bmatrix} \begin{Bmatrix} dp \\ dq \end{Bmatrix} \tag{22}$$

4.1.3 Increment equation of triaxial test

In the conventional consolidated-drained triaxial test, the stress state is in the A_3 region, and the relationship between p and q, and the relationship between the incremental dp and dq are shown in Eqs. (23)-(24), respectively:

$$p = \frac{q}{3} + \sigma_3 \tag{23}$$

$$dp = \frac{dq}{3} \tag{24}$$

For the strain-controlled triaxial test, the relationship between the axial strain increment $d\varepsilon_a$ and the volumetric strain increment $d\varepsilon_v$ is:

$$d\varepsilon_a = (d\varepsilon_s + \frac{1}{3} d\varepsilon_v) \tag{25}$$

Substituting Eq. (24) into Eq. (22), the volumetric strain increment is obtained as:

$$d\varepsilon_v = \left(\frac{1}{3}A_1 + A_2\right) dq \tag{26}$$

By substituting Eqs. (25)-(26) into Eq. (22), the axial strain increment is:

$$d\varepsilon_a = \left(\frac{1}{9}A_1 + \frac{1}{3}A_2 + \frac{1}{3}A_3 + A_4\right) dq \tag{27}$$

Simultaneous Eqs. (22) (26) (27). It is an incremental constitutive equation considering the relationship of deviatoric stress-axial strain-volumetric strain of the soil under confining pressure, including c, φ, M_1, h, t, k, n, M_2 and a total of 9 parameters.

4.2 Function expression of model parameters

According to the deviatoric stress-axial strain-volumetric strain relationship of the consolidated-drained triaxial test, the change rule of the model parameters with the number of freeze-thaw cycles N and the corresponding regression relationship, i.e., $c(N)$, $\varphi(N)$, $M_1(N)$, $h(N)$, $t(N)$, $k(N)$, $n(N)$, $M_2(N)$, $a(N)$.

4.2.1 Determination of c(N) and φ(N)

The method of determining the shear strength index is to draw the molar stress circle according to the stress path method, with $(\sigma_1+\sigma_3)/2$ as the abscissa and $(\sigma_1-\sigma_3)/2$ as the ordinate. Then, a straight line is drawn through each dome point, and the internal friction angle and cohesion are calculated according to the inclination of the straight line and its intercept on the longitudinal axis, i.e.,

$$\varphi = sin^{-1}(tan\alpha) \tag{28}$$

$$c = d/cos\varphi \tag{29}$$

In the formula, α is the inclination angle of the envelope, and d is the intercept of the longitudinal axis of the envelope.

The results of the shear strength index are shown in Table 5. Both the internal friction angle and the cohesion gradually decrease with the number of freeze-thaw cycles. Fit the regression relationship between the index value and the number of freeze-thaw cycles by using the logistic function, that is, Eq. (30). The results are shown in Fig. 7.

$$y = \frac{x_0 - A_1}{1 + (N/A_2)^{A_3}} + A_1 \tag{30}$$

In the formula, x_0 represents the value of the shear strength index without freeze-thaw cycles. N is the number of freeze-thaw cycles. A_1, A_2, and A_3 are the fitting parameters.

Table 5 Shear strength parameters of specimens under different freeze-thaw cycles

Freeze-thaw cycle	0	1	10	30	60	90	120
ϕ (°)	17.78	16.20	14.40	13.64	12.98	12.22	11.49
c (kPa)	63.73	60.40	56.76	54.03	51.21	50.70	49.84

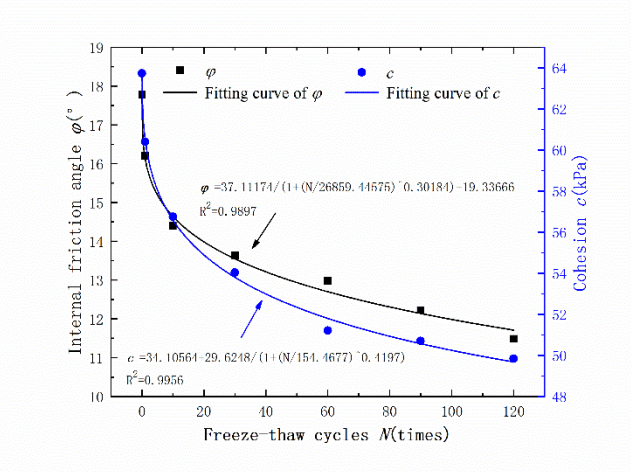

Fig. 7 Variation regularity of shear strength parameters versus number of freeze-thaw cycles

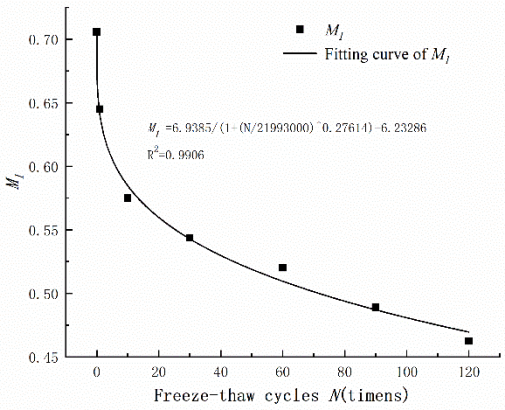

Fig. 8 Variation regularity of M_1 versus number of freeze-thaw cycles.

Table 6 Values of β、 M and M_1 under different freeze-thaw cycles

Freeze-thaw cycles	0	1	10	30	60	90	120
β	0.393	0.443	0.474	0.478	0.529	0.543	0.582
M	0.679	0.615	0.542	0.511	0.485	0.455	0.426
M_1	0.706	0.645	0.575	0.544	0.520	0.489	0.462

4.2.2 Determination of $M_1(N)$

The empirical calculation formula of $M_1(N)$ is (Yin *et al.* 1996):

$$M_1 = (1 + 0.25\beta^2)M \tag{31}$$

In the formula: β is the ratio of volumetric strain and axial strain when the stress level S_L=75%. The β value under separate confining pressures is different, and the average value is taken. For M, in the triaxial compression test, it can be obtained by Equation (32).

$$M = \frac{6sin\varphi}{3 - sin\varphi} \tag{32}$$

According to the test results, the values of β, M and M_1 are shown in Table 6. β gradually increases with the number of freeze-thaw cycles, while M and M_1 gradually decrease. The regression relationship between M_1 and the number of freeze-thaw cycles can be described by the logistic function, as shown in Fig. 8.

4.2.3 Determination of $h(N)$ and $t(N)$

The determination method of h and t is to rewrite Eq. (4) as (Yin *et al.* 1996)

$$d\varepsilon_v^p = \frac{hp_a dp_0}{(hp_a + tp_0)^2} \tag{33}$$

Let $B_p = dp_0/d\varepsilon_v^p$, and let $\Delta p_0 = p_0 - \sigma_3$, then Eq. (33) be transformed into:

$$\sqrt{\frac{B_p}{p_a}} = \sqrt{h} + \frac{t}{\sqrt{h}}\frac{p_0}{p_a} \tag{34}$$

Table 7 Values of h and t under different freeze-thaw cycles

Freeze-thaw cycles	0	1	10	30	60	90	120
h	137.640	110.229	98.835	85.182	67.437	62.323	50.046
t	1.984	2.173	2.284	2.351	2.419	2.574	2.710

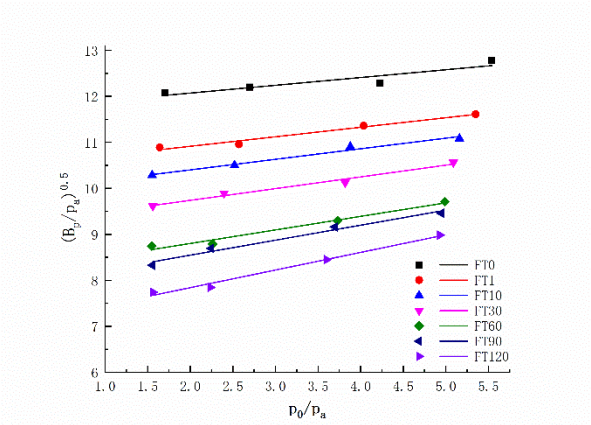

Fig. 9 Variation regularity of p_0/p_a～$(B_p/p_0)^{0.5}$ curves versus number of freeze-thaw cycles

According to application experience, the expansion strain caused by f_1 is very small among the volumetric strains caused by increasing the stress level from 0 to 50%. Approximately, it is considered to be offset by the elastic compression strain; then, the measured volume strain can be seen as the plastic volume strain ε_v^p associated with f_1. According to Eq. (2), p_0 is calculated from p and q at a stress level of 50%. Then, based on the $(B_p/p_a)^{0.5}$～p_0/p_a curves, the intercept is $h^{0.5}$ and the slope is $t/h^{0.5}$; then, h and t are obtained.

The curves of $(B_p/p_a)^{0.5}$～p_0/p_a under various freeze-thaw cycles are shown in Fig. 9, and the results of h and t are shown in Table 7. h gradually decreases with the number of freeze-thaw cycles, while t gradually increases. The regression relationship between h and t and the number of freeze-thaw cycles can be fitted by using logistic function, as shown in Fig. 10.

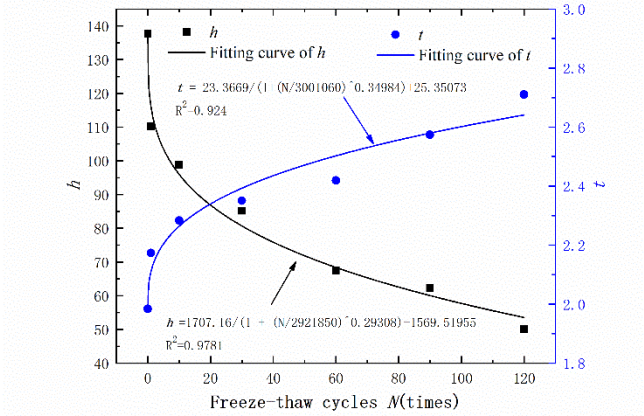

Fig. 10 Variation regularity of h and t versus number of freeze-thaw cycles

Table 8 Values of k and n under different freeze-thaw cycles

Freeze-thaw cycles	0	1	10	30	60	90	120
lgk	1.901	1.823	1.802	1.742	1.700	1.667	1.623
n	0.429	0.417	0.363	0.344	0.333	0.313	0.303
k	79.616	66.523	63.454	55.158	50.155	46.477	41.946
R^2	0.950	0.929	0.994	0.982	0.972	0.994	0.966

4.2.4 Determination of $k(N)$ and $n(N)$

$lg(\sigma_3/p_a) \sim lg(E_i/p_a)$ curves were drawn according to the stress-strain relationship, as shown in Fig. 11. As the number of freeze-thaw cycles increases, the position of the fitted line gradually decreases. The values intercept k and slope n of the straight line are shown in Table 8. Both k and n gradually decrease. The regression relationship between k and n and the number of freeze-thaw cycles can be described by logistic function, as shown in Fig. 12.

4.2.5 Determination of $M_2(N)$ and $a(N)$

The method for determining M_2 and a is to convert Eqs. (5)-(8) into (Yin *et al.* 1996):

$$\frac{p+p_r}{q} = \frac{a^2}{M_2}\left(\frac{q}{\varepsilon_s^p G}\right)^2 + \frac{1}{M_2} \tag{35}$$

Among them, the empirical formula can be used to obtain

$$\varepsilon_s^p = (0.3 - 0.1d)\varepsilon_a \tag{36}$$

In the formula, d is the slope of 75% to 95% of the stress level in the $\varepsilon_a \sim \varepsilon_v$ curve. When d is a negative value, it indicates dilatancy. The d value of each test curve is different, and the average value is taken. It is worth noting that when q is small, the value of ε_a is small, and the measurement error is also large. Therefore, when plotting the $(p+p_r)/q \sim (q/\varepsilon_s^p G)^2$ curves, only $S_L>50\%$ of the test data is used.

The point-plot $(p+p_r)/q \sim (q/\varepsilon_s^p G)^2$ curves have an intercept of $1/M_2$ and a slope of a_2/M_2 and then obtain M_2 and a. The values of M_2 and a under several freeze-thaw cycles are shown in Table 9. It can be seen that both M_2 and a gradually decrease with the number of freeze-thaw cycles,

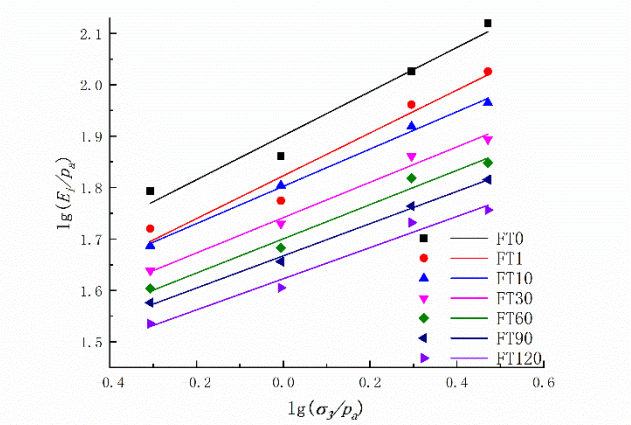

Fig. 11 Variation regularity of $lg(\sigma_3/p_a)$-$lg(E_i/p_a)$ curves versus number of freeze-thaw cycles

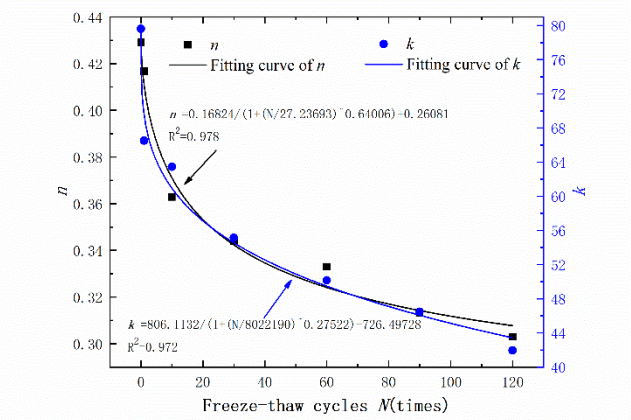

Fig. 12 Variation regularity of k and n versus number of freeze-thaw cycles

Table 9 Values of M_2 under different freeze-thaw cycles

	0	1	10	30	60	90	120
M_2	0.805	0.720	0.618	0.603	0.568	0.532	0.503
a	0.309	0.299	0.295	0.294	0.288	0.285	0.281

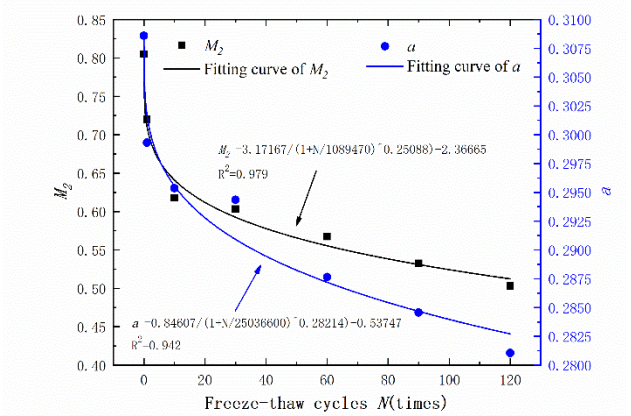

Fig. 13 Variation regularity of M_2 and a versus number of freeze-thaw cycles

and the regression relationship between the two and the number of freeze-thaw cycles can be described by the logistic function, as shown in Fig. 13.

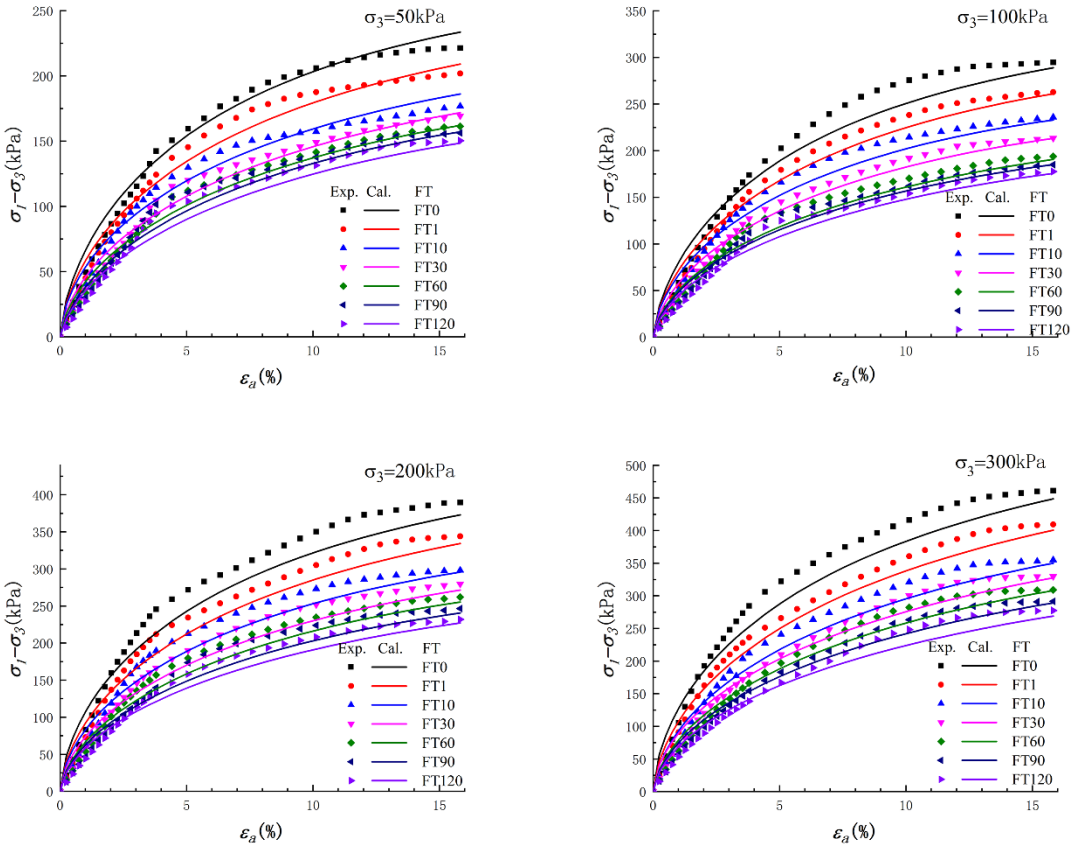

Fig. 14 Comparison between the calculated results and the experimental results of deviatoric stress-axial strain relations

5. Verification of modified double yield surface model

Based on the ellipse-parabolic double yield surface model, the model parameters are fitted to expressions with the number of freeze-thaw cycles N as the influencing factor, and a modified model considering the effects of confining pressure and freeze-thaw cycles is established. Among them, Eqs. (26)-(27) are incremental deviatoric stress-axial strain-volumetric strain deformation equations, and the calculation methods of coefficients A_1, A_2, A_3 and A_4 are Eq. (22). The calculation methods of parameters $c(N)$、$\varphi(N)$、$M_1(N)$、$h(N)$、$t(N)$、$k(N)$、$n(N)$、$M_2(N)$、$a(N)$ are shown in Fig. 7, Fig. 8, Fig. 10, Fig. 12, and Fig. 13, respectively.

Based on the Excel spreadsheet, the calculation program of the above incremental constitutive equation is compiled. The calculation process is as follows: First, according to the strain-controlled triaxial test conditions, the eccentric stress increment dq corresponding to each axial strain is calculated by Eq. (27). Then, according to dq and Eq. (26), the volumetric strain corresponding to each axial strain is calculated. Through the above calculation program, the deviatoric stress-axial strain-volumetric strain deformation relationship can be calculated under various conditions, and the results are shown in Fig. 14 and Fig. 15. The calculated results are essentially close to the measured results. When corresponding to the same axial strain, the deviator stress gradually decreases with the number of freeze-thaw cycles, and the volumetric strain gradually increases. This shows that the modified model can be used to reflect the monotonous change law of the deformation and strength characteristics of saline soil under the action of freeze-thaw cycles.

6. Conclusions

According to the experimental work of this research, under different freeze-thaw cycles (0, 1, 10, 30, 60, 90, 120) and distinct confining pressures (50, 100, 200, 300 kPa), consolidated-drained triaxial tests of the remodeled saline soils (CL) were performed, and the following main conclusions can be drawn:

- Freeze-thaw cycles play a continuous role in deteriorating the deformation and strength characteristics of saline soil. The stress-strain curves are all strain hardening types, and the appearance of the yield point is more apparent, which occurs between 3% and 5% of the axial strain. The shear strength gradually decreases with the increase in the number of freeze-thaw cycles. With the increase in the number of freeze-thaw cycles, under the first 10 freeze-thaw cycles, the shear strength declines at a greater rate, and then the decline gradually slows down. This shows that the freeze-thaw cycle still has a continuous deteriorating effect.

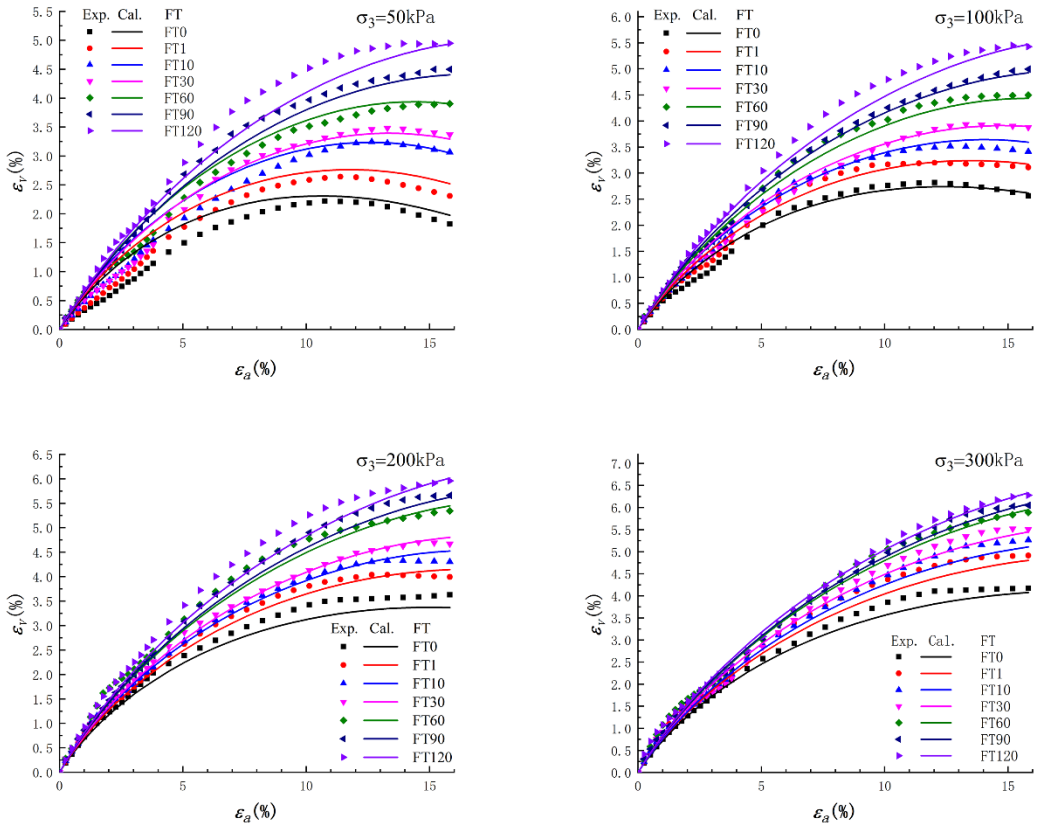

Fig. 15 Comparison between the calculated results and the experimental results of volumetric strain-axial strain relations

• As the number of freeze-thaw cycles or confining pressure increases, the volume changes in the consolidation phase and the shear phase gradually increases. The sample essentially shows shear shrinkage. Under the same test conditions, the volumetric strain gradually increases with increasing axial strain. When the confining pressure is low, the dilatation phenomenon occurs at the end of the shearing stage, and as the confining pressure and the number of freeze-thaw cycles increase, this phenomenon gradually weakens and fades.

• Based on the ellipse-parabolic double yield surface model, the correlation flow rule is introduced, and coefficient expressions between the deviating stress increment and the axial strain increment and volumetric strain increment are derived. Under the action of freeze-thaw cycles, the coefficient parameters c, φ, h, k, n, M_1, M_2 and a gradually decrease, t gradually increases, and the regression relationship between the above parameters and the number of freeze-thaw cycles can be logistic function fitting. Substitute the model parameter expression into the stress-strain increment constitutive equation to establish a modified double yield surface constitutive model considering the effects of freeze-thaw cycles.

• Compile the calculation program of the constitutive equation in the form of stress and strain increments with the number of freeze-thaw cycles and confining pressure as the influencing factors. The comparison between the calculated value and the measured value shows that the two are basically consistent, indicating that the modified elliptic -parabolic double yield surface model can be used to describe the influence of the freeze-thaw cycle on the deformation characteristics of saline soil.

Acknowledgements

This work was supported by the Key Program of International (Regional) Cooperation and Exchange of National Natural Science Foundation (Grant No. 41820104001), the Special Fund for Major Scientific Instruments of the National Natural Science Foundation of China (Grant No. 41627801) and A project funded by the Jilin Provincial Water Resources Department (Grant No.126002-2020-0001). We sincerely thank all the reviewers and editors for their professional comments and suggestions regarding this manuscript.

References

Asoka, A., Nakano, M. and Noda, T. (2000), "Super loading yield surface concept for highly structured soil behavior", *Soil. Foundation.*, **40**(2), 99-110. http://doi.org/10.3208/sandf.40.2_99.

ASTM D2487-11 (2011), Standard practice for classification of soils for engineering purposes (unified soil classification system), ASTM International; PA, USA. http://doi.org/10.1520/D2487-11

Bai, X.D., Cheng, W.C., Ong, D.E.L. and Li, G. (2021),

"Evaluation of geological conditions and clogging of tunneling using machine learning", *Geomech. Eng.*, **25**(1), 59-73. http://doi.org/10.12989/gae.2021.25.1.059.

Bao, S., Wang, Q. and Bao, X. (2013), "Study on dispersive influencing factors of dispersive soil in western Jilin based on grey correlation degree method", *Appl. Mech. Mater.*, **291-294**, 1096-1100. http://doi.org/10.4028/www.scientific.net/amm.291-294.1096.

Chang, D. and Lai, Y. (2018), "A double-yield-surface model for frozen saline sandy soil incorporating particle crushing", *Proceedings of China-Europe Conference on Geotechnical Engineering*, Vienna, August. https://doi.org/10.1007/978-3-319-97115-5_95.

Chang, D., Lai, Y. and Yu, F. (2019), "An elastoplastic constitutive model for frozen saline coarse sandy soil undergoing particle breakage", *Acta Geotechnica*, **14**, 1757-1783. https://doi.org/10.1007/s11440-019-00775-0.

Chang, D., Liu, J. and Li, X. (2015), "Experimental study on yielding and strength properies of silty sand under freezing-thawing cycles", *Chinese J. Rock Mech. Eng.*, **34**(8), 1721-1728. http://doi.org/10.13722/j.cnki.jrme.2014.1643.

Chang, D., Liu, J. and Li, X. (2016), "A constitutive model with double yielding surfaces for silty sand after freeze-thaw cycles", *Chinese J. Rock Mech. Eng.*, **35**(3), 623-630. https://doi.org/10.13722/j.cnki.jrme.2015.0505.

Chen, Z. and Zhu, J. (2016), "A modified ellipse-parabola double yield surfaces model on gravelly soil", *J. Fuzhou University* (*Natural Science Edition*), **44**(6), 874-880. http://doi.org/10.7631/issn.1000-2243.2016.06.0874.

Cheng, W.C., Duan, Z., Xue, Z.F. and Wang, L. (2021), "Sandbox modelling of interactions of landslide deposits with terrace sediments aided by field observation", *Bulletin Eng. Geology Environ.*, **80**(4), 3711–3731. https://doi.org/10.1007/s10064-021-02144-2.

Cui, H., Liu, J., Zhang, L. and Tian, Y. (2015), "A constitutive model of subgrade in a seasonally frozen area with considering freeze-thaw cycles", *Rock Soil Mech.*, **36**(08), 2228-2236. http://doi.org/10.16285/j.rsm.2015.08.014.

Duncan, J.M. and Chang, C.Y. (1970), "Nonlinear analysis of stress and strain in soils", *J. Soil Mech. Foundation Division*, **96**(5), 1629-1653. https://doi.org/10.1061/JSFEAQ.0001458.

Han, Y., Wang, Q., Wang, N., Wang, J., Zhang, X., Cheng, S. and Kong, Y. (2018), "Effect of freeze-thaw cycles on shear strength of saline soil", *Cold Regions Sci. Technol.*, **154**, 42-53. https://doi.org/10.1016/j.coldregions.2018.06.002.

Hu, T., Liu, J., Wang, T. and Yue, Z. (2019), "Effect of freeze-thaw cycles on the deformation characteristics of a silty clay and its constitutive model with double yielding surfaces", *Rock Soil Mech.*, **40**(3), 987-997. https://doi.org/10.16285/j.rsm.2017.1829.

Hu, W., Cheng, W.C., Wen, S. and Rahman, M.M. (2021), "Effects of chemical contamination on microscale structural characteristics of intact loess and resultant macroscale mechanical properties", *CATENA*, **203**. https://doi.org/10.1016/j.catena.2021.105361.

Huang, M., Hu, P. and Zhang, H. (2008), "Two-yield surface constitutive model for fine sand in consideration of dilatancy and strain softening", *J. Hydraulic Eng.*, **39**(2), 129-136. http://doi.org/10.3321/j.issn:0559-9350.2008.02.001.

Huang, W., Pu, J. and Chen, Y. (1981), "Hardening rule and yield function for soils", *Chinese J. Geotech. Eng.*, **3**, 19-26.

Kong, Y., Xu, M. and Song, E. (2017), "An elastic-viscoplastic double-yield-surface model for coarse-grained soils considering particle breakage", *Comput. Geotech.*, **85**, 59-70. http://doi.org/10.1016/j.compgeo.2016.12.014.

Lade, P.V. (1977), "Elasto-plastic stress-strain theory for cohesionless soil with curved yield surfaces", *Int. J. Solids Struct.*, **13**(11), 1019-1035. http://doi.org/10.1016/0020-7683(77)90073-7.

Lai, Y., Jin, L. and Chang, X. (2009), "Yield criterion and elasto-plastic damage constitutive model for frozen sandy soil", *Int. J. Plasticity*, **25**(6), 1177-1205. http://doi.org/10.1016/j.ijplas.2008.06.010.

Lai, Y., Yang, Y., Chang, X. and Li, S. (2010), "Strength criterion and elastoplastic constitutive model of frozen silt in generalized plastic mechanics", *Int. J. Plasticity*, **26**(10), 1461-1484. https://doi.org/10.1016/j.ijplas.2010.01.007.

Lai, Y.M., Xu, X.T., Yu, W.B. and L., Q.J. (2014), "An experimental investigation of the mechanical behavior and a hyperplastic constitutive model of frozen loess", *Int. J. Eng. Sci.*, **84**, 29-53. https://doi.org/10.1016/j.ijengsci.2014.06.011.

Li, G. (2006), "Characteristics and development of tsinghua elasto-plastic model for soil", *Chinese J. Geotech. Eng.*, **28**(1), 1-10. http://doi.org/10.1016/S1872-1508(06)60035-1.

Li, S., Niu, F., Lai, Y., Pei, W. and Yu, W. (2017), "Optimal design of thermal insulation layer of a tunnel in permafrost regions based on coupled heat-water simulation", *Appl. Thermal Eng.*, **110**, 1264-1273. http://doi.org/10.1016/j.applthermaleng.2016.09.033.

Li, X. and Dafalias, Y.F. (2000), "Dilatancy for cohesionless soils", *Geotechnique*, **50**, 449-460. http://doi.org/10.1680/geot.2000.50.4.449.

Liu, J., Chang, D. and Yu, Q. (2016), "Influence of freeze-thaw cycles on mechanical properties of a silty sand", *Eng. Geology*, **210**, 23-32. https://doi.org/10.1016/j.enggeo.2016.05.019.

Liu, J., Lv, P., Cui, Y. and Liu, J. (2014), "Experimental study on direct shear behavior of frozen soil–concrete interface", *Cold Regions Sci. Technol.*, **104-105**, 1-6. http://doi.org/10.1016/j.coldregions.2014.04.007.

Liu, M., Liu, H. and Gao, Y. (2012), "New double yield surface model for coarse granular materials incorporating nonlinear unified failure criterion", *J. Central South U.*, **19**(11), 3236-3243. https://doi.org/10.1007/s11771-012-1400-z.

Roscoe, K. and Schofield, A. (1963), "Mechanical behaviour of an idealised 'wet-clay'", *Proceedings of the European Conference on Soil Mechanics and Foundation Engineering*, Wiesbaden, October, 47-54.

Shen, Z. (1980), "The rational form of stress-strain relationship of soils based on elasto-plasticity theory", *Chinese J. Geotech. Eng.*, **2**(2), 11-19.

Suebsuk, J., Horpibulsuk, S. and Liu, M.D. (2019), "Compression and shear responses of structured clays during subyielding", *Geomech. Eng.*, **18**(2), 121-131. https://doi.org/10.12989/gae.2019.18.2.121.

Sukkarak, R., Pramthawee, P. and Jongpradist, P. (2016), "A modified elasto-plastic model with double yield surfaces and considering particle breakage for the settlement analysis of high rockfill dams", *KSCE J. Civil Eng.*, **21**(3), 1-12. http://doi.org/10.1007/s12205-016-0867-9.

Wang, Q., Kong, Y., Zhang, X., Ruan, Y. and Chen, Y. (2016), "Mechanical effect of pre-consolidation pressure of structural behavior soil", *J. Southwest Jiaotong U.*, **51**(5), 987-994. http://doi.org/10.3969/j.issn.0258-2724.2016.05.023.

Wang, S., Wang, Q., Qi, J. and Liu, F. (2018), "Experimental study on freezing point of saline soft clay after freeze-thaw cycling", *Geomech. Eng.*, **15**(4), 997-1004. http://dx.doi.org/10.12989/gae.2018.15.4.997.

Yang, D., Yan, C., Liu, S., Zhang, J. and Hu, Z. (2019), "Stress-strain constitutive model of concrete corroded by saline soil under uniaxial compression", *Construct. Building Mater.*, **213**, 665-674. https://doi.org/10.1016/j.conbuildmat.2019.03.153.

Yao, Y. (2015), "Advanced UH models for soils", *Chinese J. Geotech. Eng.*, **37**(2), 193-217. http://doi.org/10.11779/CJGE201502001.

Yao, Y., Zhang, B. and Zhu, J. (2012), "Behaviors , constitutive model sand numerical simulation of soils", *China Civil Eng. J.*, **45**(3), 135-158.

Yin, Z. (1988), "A stress-strain model of soil with double yield surfaces", *Chinese J. Geotech. Eng. Geology*, **10**(4), 66-73.

Yin, Z., LU, H. and Zhu, J. (1996), "The elliptic-parabolic yield surfaces model and its softness matrix", *J. Hydraulic Eng.*, **12**(12), 23-28.

Yu, F., Qi, J., Zhang, M., Lai, Y., Yao, X., Liu, Y. and Wu, G. (2016), "Cooling performance of two-phase closed thermosyphons installed at a highway embankment in permafrost regions", *Appl. Thermal Eng.*, **98**, 220-227. http://doi.org/10.1016/j.applthermaleng.2015.11.102.

Zhang, M., Lai, Y., Li, D., Tong, G. and Li, J. (2012), "Numerical analysis for thermal characteristics of cinderblock interlayer embankments in permafrost regions", *Appl. Thermal Eng.*, **36**, 252-259. http://doi.org/10.1016/j.applthermaleng.2011.10.020.

Zhang, X., Ren, K., Sun, H., Xing, Y. and Yang, J. (2018), "Constitutive relationship with double yield surfaces for cinder improved soil under freeze-thaw cycles", *Chinese J. Rock Mech. Eng.*, **37**(8), 1916-1923. http://doi.org/10.13722/j.cnki.jrme.2018.0129.

Zhang, X., Wang, Q., Li, P. and Wang, R. (2015), "Research on soil dispersion of qian'an soil forest", *J. Northeastern U. (Natural Science)*, **36**(11), 1643-1647. http://doi.org/10.3969/j.issn.1005-3026.2015.11.027.

Zhang, X., Zhai, E., Sun, D.A., Wu, Y. and Lu, Y. (2021), "Theoretical and numerical analyses on hydro–thermal–salt–mechanical interaction of unsaturated salinized soil subjected to typical unidirectional freezing process", *Int. J. Geomech.*, **21**(7), https://doi.org/10.1061/(ASCE)GM.1943-5622.0002036.

Zhao, B., Huang, T., Liu, D., Liu, Y., Wang, X., Liu, S. and Yu, G. (2019), "Study on the mechanical properties test and constitutive model of rock salt", *Geomech. Eng.*, **18**(3), 291-298. http://dx.doi.org/10.12989/gae.2019.18.3.291.

Zhao, Y., Lai, Y., Pei, W. and Yu, F. (2020), "An anisotropic bounding surface elastoplastic constitutive model for frozen sulfate saline silty clay under cyclic loading", *Int. J. Plasticity*, **129**(4), 102668. https://doi.org/10.1016/j.ijplas.2020.102668.

Zhou, C.Y. and Zhu, F.X. (2010), "An elasto-plastic damage constitutive model with double yield surfaces for saturated soft rock", *Int. J. Rock Mech. Mining Sci.*, **47**(3), 385-395. http://doi.org/10.1016/j.ijrmms.2010.01.002.

Zhou, G., Hu, K., Zhao, X., Wang, J. and Lu, G. (2015), "Laboratory investigation on tensile strength characteristics of warm frozen soils", *Cold Regions Sci. Technol.*, **113**. http://doi.org/10.1016/j.coldregions.2015.02.003.

Zhu, Z., Kang, G., Ma, Y., Xie, Q., Zhang, D. and Ning, J. (2016), "Temperature damage and constitutive model of frozen soil under dynamic loading", *Mech. Mater.*, **102**, 108-116. http://doi.org/10.1016/j.mechmat.2016.08.009.

CC